Shape, orientation relationships and interface structure of beta-Nb nano-particles in neutron irradiated zirconium alloy

J. Ribis[1*], S. Doriot[1] F. Onimus[1]

[1] DEN-Service de Recherches Métallurgiques Appliquées, CEA, Université Paris-Saclay, F-91191, Gif-sur-Yvette, France
*Corresponding author: J. Ribis Tel (33) 1 69 08 85 09, joel.ribis@cea.fr

Abstract

Under neutron irradiation, radiation enhanced beta-Nb nano-precipitates develop within the α-grains of the Zr-Nb alloys. This radiation enhanced precipitation is of great interest since it may have some influence on the post-irradiation mechanical behavior of the material. In this paper the shape, the orientation relationship and the interface structure of such nano-particles are studied by means of both conventional and high-resolution transmission electron microscopy. The radiation damage was annealed out, thanks to a prior heat treatment and a creep test, in order to easily observe the beta-Nb nano-particles. The nano-particles exhibit a needle-like shape with a short thickness along the c-direction of 1.5 nm on average, a length and a width respectively of 6 nm and 3 nm, on average, in the basal plane. Using high-resolution TEM, a near Pitsch-Schrader orientation relationship is identified for a nano-particle. The interface atomic structure at various locations around the nano-particle has been accurately determined and an atomic model of the interface structure has been proposed.

Introduction

Zirconium alloys are commonly used in Pressurized Water Reactors, as cladding tubes of the nuclear fuel owing to their excellent properties for nuclear applications. In-reactor, the components made of zirconium alloys are subjected to high irradiation doses. Hence, the understanding of neutron irradiation effects on zirconium alloys is an important step toward the prediction of the integrity of these components. Among the wide variety of zirconium alloys, the Zr-Nb alloys are extensively used for their good corrosion resistance [1, 2, 3].

In the M5[TM] alloy, which contains 1%wt of Nb, part of the Nb atoms are in substitutional solid solution. Because the solubility limit of Nb in alpha-Zr is always lower than 1%wt [2, 4] the remaining Nb atoms form a homogeneously refined dispersion of beta-Nb precipitates [6]. These native beta-Nb precipitates have the size of 50 nm and a b.c.c. lattice with the parameter a = 0.328 nm [5].

In fact, after processing, the concentration of Nb in solid solution in the Zr matrix corresponds to the maximum solubility near the monotectoid temperature, which is higher than the solubility at the service temperature (350°C). Owing to the slow diffusion of Nb, the equilibrium microstructure cannot be reached thermally during the cooling down after the heat treatment. The alpha-Zr matrix therefore exhibits a slight super-saturation of Nb atoms. As pointed out in [7], only very long term annealing

treatments (up to 20000 hours) allow reaching the thermodynamics equilibrium at temperatures below 580°C.

Interestingly, after a few years in reactors, a high density of nano-precipitates is observed [6, 8, 9]. These nano-precipitates are usually imaged using the g=0002 diffraction vector. In this condition, the numerous and small <a>-loops disappear, allowing an easy observation of other microstructural features such as the nano-precipitates. According to Doriot et al. [6], the nano-particles look circular, with diameter close to 3 nm for fluences lower than 3×10^{25} n/m^2, and are randomly dispersed. For further irradiation dose, they gradually tend to concentrate within 50 nm spaced layers parallel to the basal plane, and some of them become elongated in the direction close to the basal plane trace. The average width of these needle shaped precipitates is between 1 to 3 nm and the length increases up to 12 nm (6 nm long on average) [10, 11, 12]. This very peculiar shape has to be attributed to the effect of irradiation since, after thermal annealing only, for 1500 hours at temperature up to 770 K, this shape and size of beta-Nb precipitate is never observed [13]. It is also shown that these nano-precipitates are thermodynamically stable since they do not disappear after annealing, at least after heat treatments up to 770 K [10]. This suggests that they result from the radiation-enhanced diffusion of Nb due to the high concentration of vacancies under irradiation [8]. Indeed, since the as-received Zr-1%Nb alloy consists in a α-phase matrix supersaturated in Nb atoms, in addition to the native beta-Nb globural precipitates [14], the irradiation conducted below the monotectoid temperature leads to the precipitation of the supersaturated Nb, as predicted by the phase diagram.

EDX analyzes on extraction replica have measured a composition of about 60%wt Nb for these needle-shape nano-particles. This niobium content of 55-60% is similar to that of native beta-Nb particles irradiated at high fluences and is supposed to be the "equilibrium" composition of these particles under irradiation [15]. It should be pointed out herein that, based on the binary phase diagram [16, 17], the equilibrium content of Nb in beta-Nb should be close to 91% at operating temperature. This suggests that the "equilibrium" composition under irradiation is not the thermodynamic equilibrium. Recently, these beta-Nb needle-shape nano-particles have been analyzed using synchrotron diffraction [10]. The diffraction peaks were consistent with BCC beta-Nb. Despite the difficulty for the T-XRD signal de-convolution and despite the possible elastic strain in these nano-precipitates that can modify the crystallographic parameters, the Nb content in these particles was evaluated from the measurement of the lattice parameter, using the Vegard's law, and was about 60% (lattice parameter a=3.4150 A) up to 2 PWRs irradiation cycles.

Sarce [18] explained, using the Maydet and Russel approach [19], the peculiar shape of these nano-precipitates by the assumed anisotropic diffusion of point defects. Nevertheless, Sarce [18] based its theoretical results on the hypothesis that beta-Nb particles are incoherent with the matrix while according to Turkin et al. [20], the beta-Nb particles are only partly coherent with the α-matrix. Turkin et al. [20] attributed the form of needles to the large interface energy. According to Turkin et al. [20], most of the interface of such a precipitate is coherent with the matrix, while the lattice misfit is accommodated at incoherent zones of the interface, which are small compared to the coherent ones.

The 3D geometry, the detailed interface structure and the Orientation Relationship (OR) of the beta-Nb nano-precipitates are topics of interest since these nano-precipitates may play a role on the post-irradiation mechanical properties of Zr-Nb alloys. Indeed, these nano-precipitates contribute to the remaining hardening observed after annealing out the irradiation damage, as pointed out in [21, 22,

23]. They also may play a role on the post-irradiation creep behavior, when irradiation damage annealing occurs, during the back-end cycles, such as transportation and dry storage of the fuel assembly.

In order to bring new insights on the beta-Nb nano-particles and their potential role on the post-irradiation mechanical behavior, a neutron irradiated sample made of Zr-1%Nb alloy, which has undergone first a heat treatment and then a creep test, has been studied. The beta-Nb nano-precipitates were analyzed using conventional TEM imaging and High Resolution Transmission Electron Microscopy (HRTEM).

Material and experimental details

The studied material is a Zr-1%Nb alloy, namely M5®, which is in a recrystallized metallurgical state [3]. This material is characterized by 6 µm size equiaxed grains with a strong crystallographic texture. The second phase particles are mainly 50 nm diameter spherical beta-Nb precipitates homogeneously dispersed throughout the grains.

The chemical composition (in wt%) of this commercial alloy is given in Table 1. This material has been irradiated as cladding tube in a PWR power plant at operating temperature of 623 K up to a fluence of 1.1×10^{26} $n.m^{-2}$ (E> 1MeV). After use, the cladding tube was cut, defueled and then several thermomechanical treatments were performed in order to study the behavior of the material. First a heat treatment was conducted at 723 K during 960 hours, then, an internal pressure creep test was performed on the cladding at 673 K with an applied hoop stress equal to 130 MPa during 960 hours. During these thermal treatment, there was a possible modification of the needle-like particle composition in order to reach the thermodynamic equilibrium composition. The results of the mechanical tests are not shown here, as the present paper focuses on the microstructure of the material. After testing, TEM thin foils were prepared in hot cell. Small tiles were cut out, mechanically-polished down to a thickness of 100 µm, then 3 mm disks were punched out, and jet-polished using Ethanol/Perchloric acid solution at 278 K.

Table 1. Chemical composition of the Zr-1%Nb alloy

Element	Nb	Fe	O	Zr
M5®	1.00	0.03	0.12	Balance

TEM method

Conventional TEM was firstly conducted on a JEOL 2100 TEM operating at 200 kV. Two different imaging conditions were used: the nano-precipitates were observed in grains orientated with the electron beam in the basal plane, the basal plane being edge-on, using a diffraction vector along the c-axis (g=0002). This imaging condition corresponds to the usual condition to observe c-component loops and also the beta-Nb nano-precipitates. Indeed, after irradiation inside a PWR, the material contains a very high density of small a-loops that impede the observation of other microstructural features. By using the g=0002 diffraction vector all the a-loops are then extinguished. However, thanks to the heat treatment conducted on the sample used in this study, the a-loops have been annealed

out so that beta-Nb nano-precipitates can be observed in any other orientations. The nano-precipitates were then observed in grains with the <c> axis close to the electron beam allowing the study of the 3D geometry of these precipitates.

Furthermore, thanks to the annealing of the a-loops, it is easier to perform High Resolution Transmission Electron Microscopy on these precipitates. Indeed, due to the strong texture of the material, the large majority of the grains have the c-axis close to the foil normal. Because here the loops have been annealed out, the nano-precipitates can be easily observed in the thinnest area of these grains with only low tilt angles. The high resolution transmission electron microscopy was performed on a JEOL 2010F field emission gun microscope operating at 200 kV.

Results :

Nano beta-Nb particles observed by conventional TEM imaging

The Figure 1 shows a grain oriented with the zone axis $[1\bar{1}00]$ close to the electron beam. The picture in figure 1(a) was obtained using the diffraction vector $g=11\bar{2}0$, and the picture in figure 1(b) was obtained using the diffraction vector $g=0002$. In figure 1(c), is shown a detailed overlap of the various microstructural features that can be found in the material (a-dislocations, c-loops, nano-precipitates). First it is worth pointing out that the a-loops have been completely annealed out, resulting from the significant heat treatment applied to the material (960 hours at 723 K then 960 hours at 673 K). Linear a-dislocations are observed resulting from the deformation during the creep test (960 hours at 673K under 130 MPa hoop stress). Moreover, in figure 1(b), c-component loops are observed along with the nano-precipitates.

These precipitates exhibit a needle-like shape, observed edge-on, and furthermore they show alternate layers depleted from precipitates and layers with aligned precipitates. The width of these nano-precipitates, measured on this picture, is between 1 to 3 nm, the average width being 1.5 nm. The length of the needle shape precipitates is in between 2 nm to 15 nm, for the longest, the average length being 5 nm. The distance between two layers of nano-precipitates is between 40 nm to 70 nm and on average 50 nm on this picture.
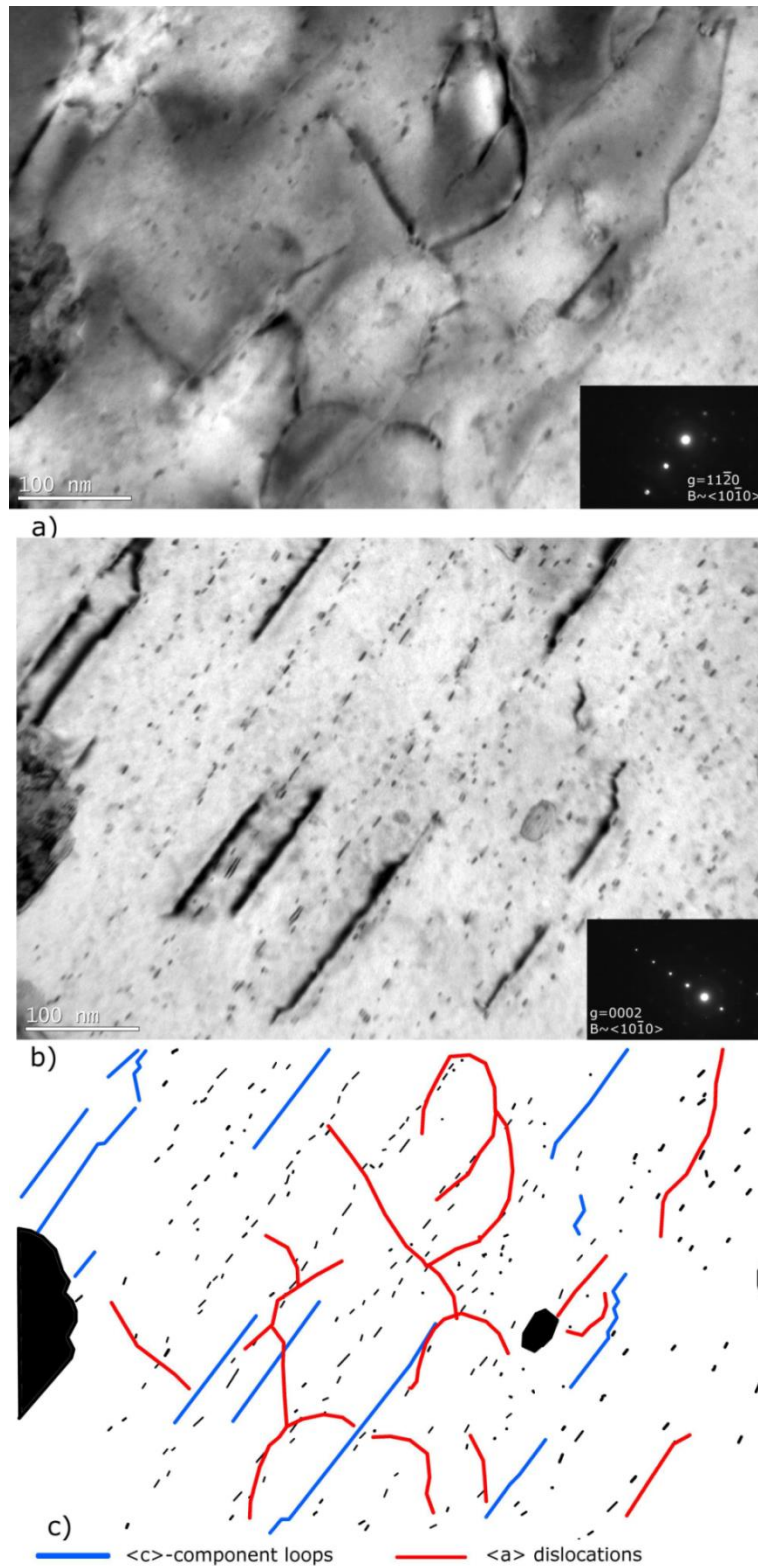
Figure 1 : TEM micrographs of a grain with the zone axis B~[10$\bar{1}$0] close to the electron beam a) picture obtained with diffraction g=1$\bar{1}$20, b) picture obtained with a diffraction g=0002. c) Detailed drawing showing the overlap of c-loops, a-dislocations and beta-Nb nano-precipitates.
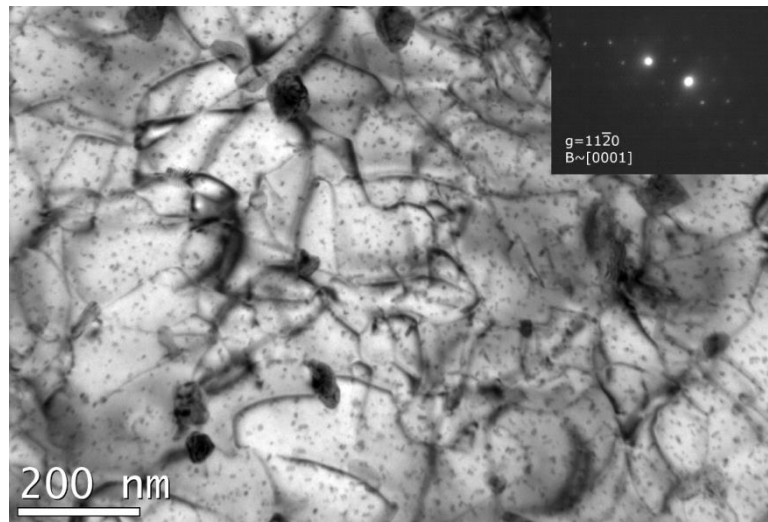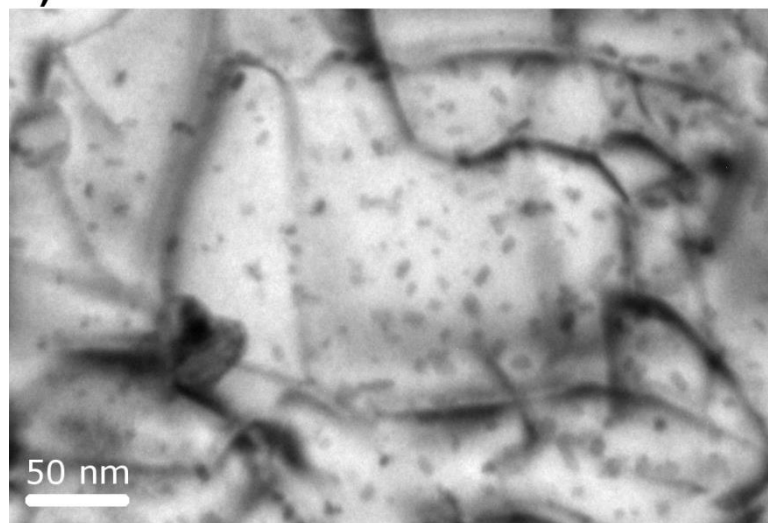
Figure 2 : **a) Imaging of nano-precipitates and dislocation with a diffraction vector $\underline{g}$=11$\overline{2}$0 and the electron beam close to the zone axis $\underline{B}$~[0002]. The corresponding diffraction pattern is shown encapsulated. b) a zoom on the center of the picture is also shown. c) Detailed drawing showing the dislocations and beta-Nb nano-precipitates.**

The Figure 2 shows a grain oriented with the zone axis [0002] close to the electron beam. Using the diffraction vector g=11$\bar{2}$0, entangled a-dislocations and numerous nano-precipitates can be observed. C-component dislocation loops are also present although not distinguished from a-dislocations. An enlarged view of the center of the picture is shown in figure 2b.

The nano-precipitates exhibit a slight acicular shape, the width being at maximum 5 nm and on average 3 nm wide. The length of the precipitates, in this picture, is at maximum 15 nm and on average 7 nm. The orientation of the long direction of the particles seems nearly random in the basal plane.

Based on the observation of these precipitates along two perpendicular points of view, it can be concluded that these particles have, on average, the 3D geometry of small flattened needles (or flattened rice grain), the long direction (6 nm) and the width (3 nm) of the needles are in the basal plane, the short thickness (1.5 nm) being along the <c> axis (Figure 3).

It could also be stressed that the fact that these nano-precipitates are clearly observed after a significant heat treatment (960 hours at 723 K then 960 hours at 673 K) shows that these precipitates are thermodynamically stable.
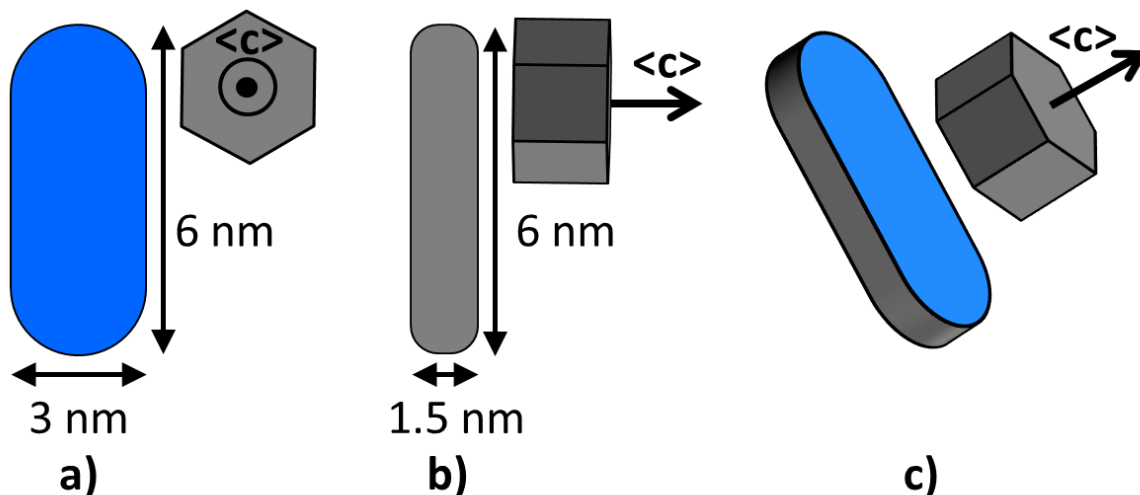
Figure 3 : Schematic of a beta-Nb nano-precipitate a) observed with the electron beam parallel to the <c> axis, b) observed with the electron beam in the basal plane. c) 3D geometry of the nano-precipitate.

Atomic structure beta-Nb particles

High resolution transmission electron microscopy was then conducted on very thin areas of the same sample using only small tilt angles, that is, with the electron beam close to [0001] zone axis of the zirconium matrix beacause of the strong texture of the material. In order to determine the lattice structure parameter and symmetry of beta-Nb nano-particles, three high resolution patterns were acquired on three distinct particles. The results are shown in figure 4. The three particles are observed along the <001> (figure 4 (a)), <011> (figure 4 (b)) and <111> (figure 4 (c)) zone axis. For the first particle, shown in figure 4 (a), the d{100} and d{110} interplanar distances are found to be equal to

0.33 and 0.23 nm respectively. For the second particle, observed along the <011> zone axis (figure 4 (b)), the d{100} is measured at the same values than measured previously whereas the d{110} is slightly higher since it is found to be equal to 0.27 nm. Finally, concerning the third particle observed along the <111> zone axis (figure 4 (c)), the d{110} is also found to be equal to 0.27 nm.

Figure 5 gives a comparison between experimental high resolution images along the <001>, <110> and <111> zone axis (figure 5 (a), (c), (e)) and the corresponding simulated high resolution images using a multislice method [23] (figure 5 (b), (d), (f)). The Nb structure has been simulated by considering the Im$\bar{3}$m space group. The results (figure 5) show a perfect matching between experimental and processed high resolution images which strongly suggests that the structure of the beta-Nb particles is consistent with the Nb equilibrium Im$\bar{3}$m structure. However, in some cases a deviation from the theoretical value of the d{110} interplanar distance is reported and will be discussed later.
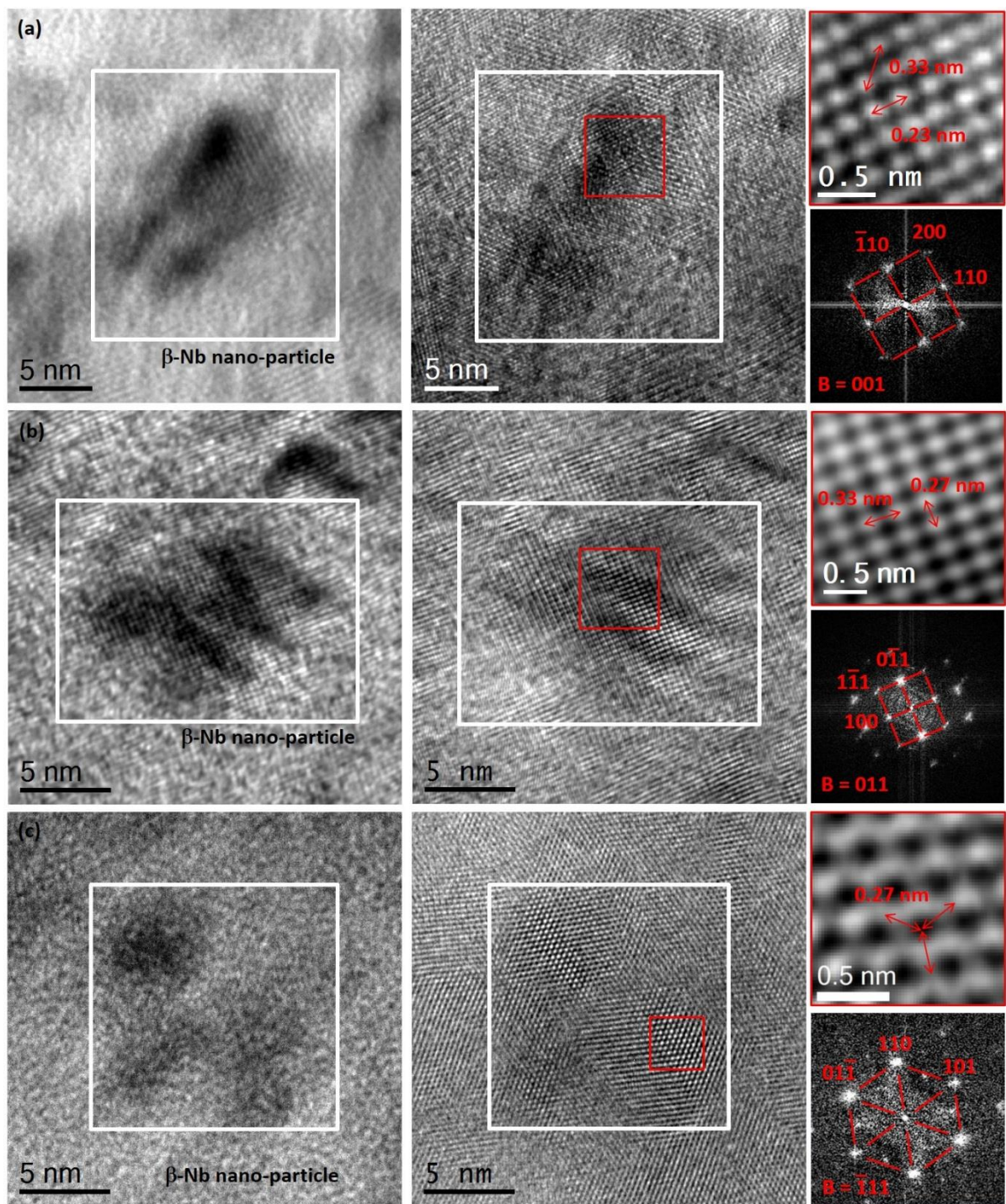
Figure 4: Identification of the lattice structure of the beta-Nb by HRTEM : (a) beta-Nb oriented along the <001> zone axis, (b) beta-Nb oriented along the <011> zone axis, (c) beta-Nb oriented along the <111> zone axis.

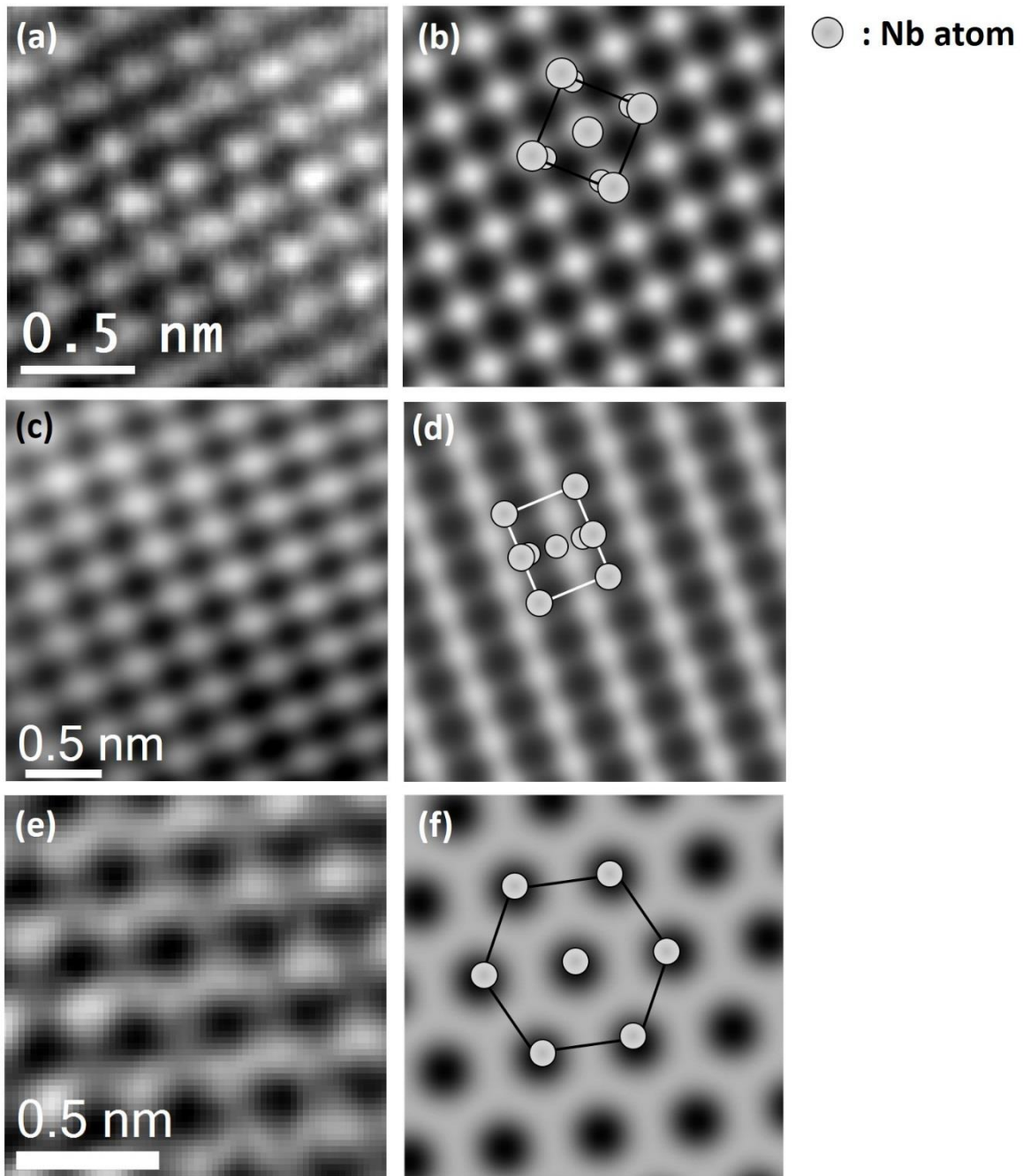**Figure 5: High-resolution TEM image simulation using the theoretical Im-3m b.c.c structure with lattice parameter equal to 0.33 nm: (a) HRTEM image along the <001> zone axis, (b) simulation of the b.c.c. structure along the <001> zone axis, (c) HRTEM image along the <011> zone axis, (d) simulation of the b.c.c. structure along the 011 zone axis, (e) HRTEM image along the <111> zone axis, (f) simulation of the b.c.c. structure along the <111> zone axis (defocus = 5 nm and thickness = 5 nm).**

Orientation relationships with the matrix

The Orientation Relationships of a needle-shaped particle with the matrix was identified by means of high resolution TEM. Figure 6 (a) shows bright-field TEM micrograph of a nano-particle while figure 6 (b) is a high resolution TEM micrograph of the same particle and figure 6 (c) is the corresponding FFT. For this particle, the FFT agrees well with a near Pitsch-Schrader OR (i.e. $(0001)//(011)$ and $[11\bar{2}0]//[100]$). In our case, the $[\bar{1}2\bar{1}0]$ is $\sim2°$ from $[\bar{1}00]$, the $[\bar{1}010]$ is $\sim2°$ from $[0\bar{1}1]$, and the $[11\bar{2}0]$ is $\sim4°$ from $[\bar{1}1\bar{1}]$. The long axis of this particle is parallel to the $[\bar{1}\bar{1}20]$ direction. The stereographic projections corresponded to this OR is given in figure 7.

Atomic-scale images (figure 6 (d)) obtained along the common zone axes of the two crystals of niobium and zirconium allow to precisely define the atomic structure of the resulting interface. The atomic configurations of the different interfaces produced by this OR are thus described hereafter.
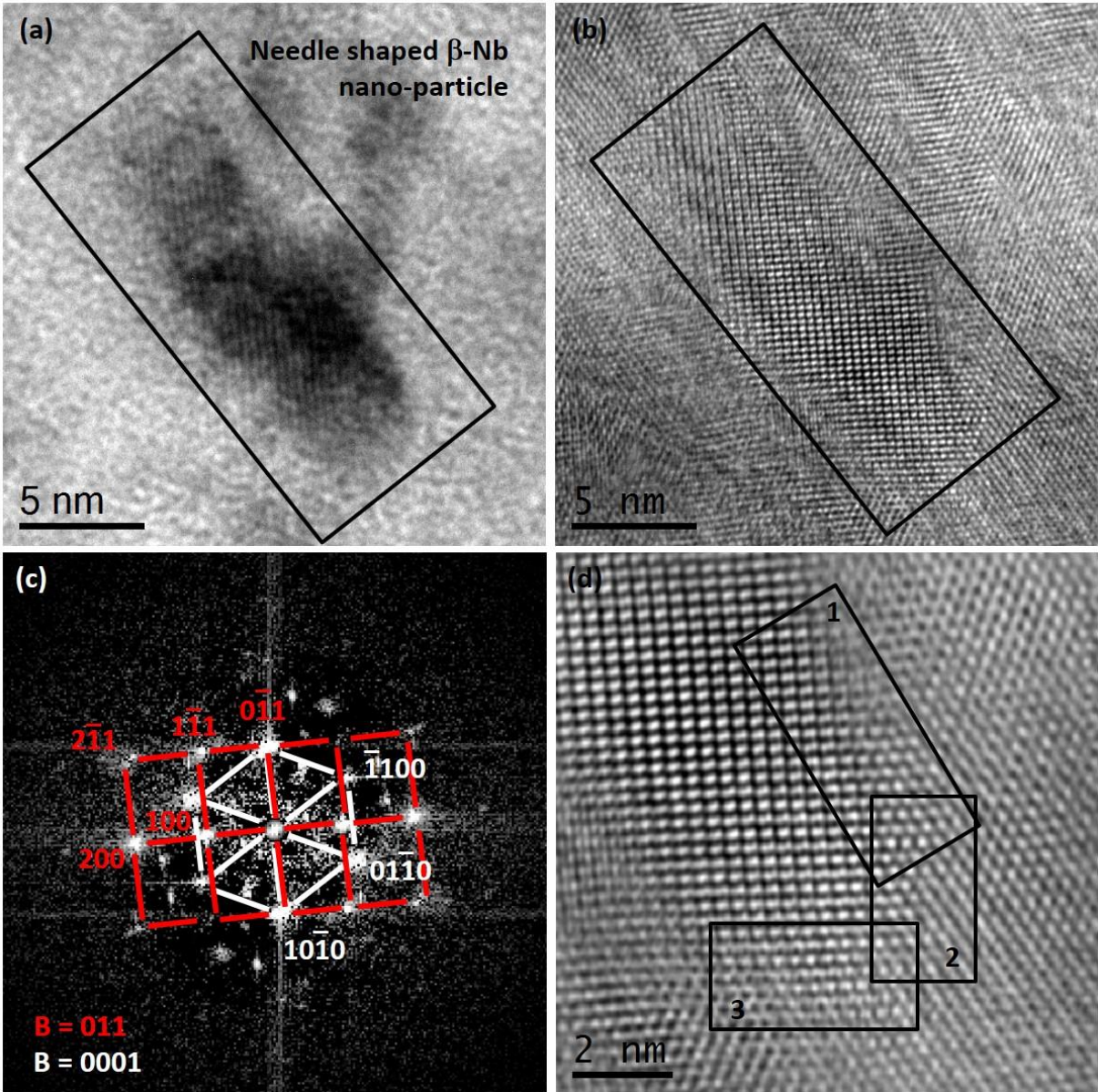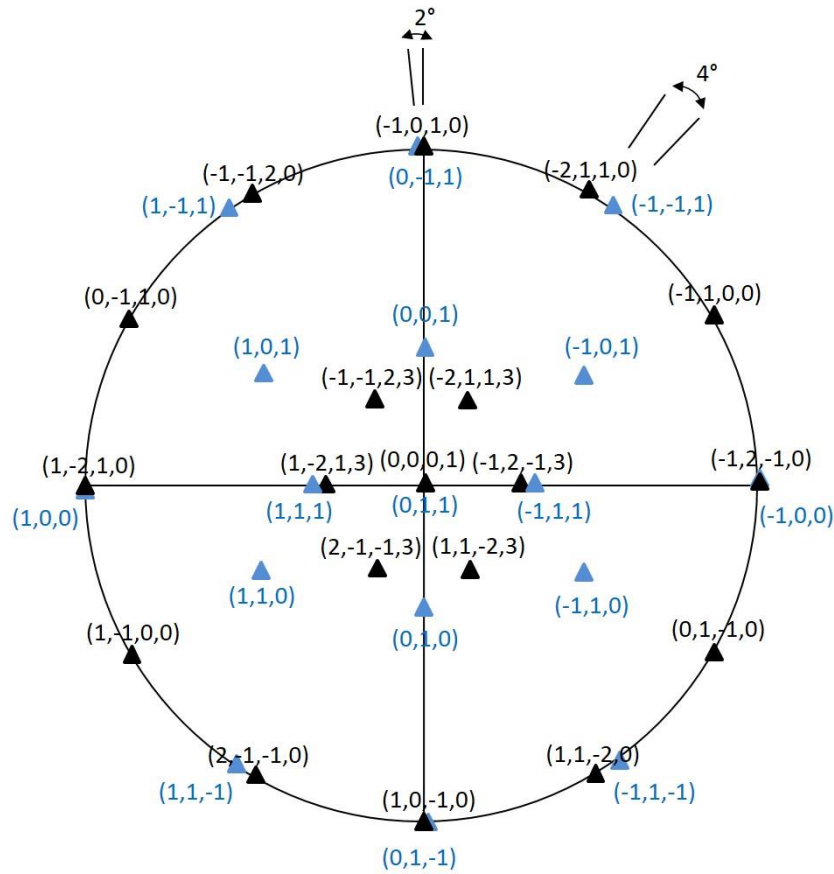
Figure 6: Orientation relationships of a needle-shaped precipitate: (a) bright-field micrograph, (b) high-resolution micrograph, (c) corresponding FFT, (d) interface structure. The zones 1, 2 and 3 are analyzed on figure 9 and 10.

Figure 7: Stereographic projection of the particle observed in figure 6.

Atomic Interface structure

Figure 6 (d) is a high resolution image of a nano-particle where white dots represent atomic columns in both Zr and Nb crystals. The interface of the particle has been divided in three parts. The long interface of the particle labelled 1 (top of figure 6(d)), the interface labelled 2 (right part of Figure 6(d)) and the interface labelled 3 (bottom of figure 6 (d)). The three interfaces are shown at high magnification in figure 8 (a, c and e) respectively. Atomic models of the structure of these three interfaces, are proposed in figure 9 (a, b and c). From these atomic models, high resolution images have been simulated by using the "crystalkit" software [25] and a multislice method [24]. A correct matching between simulated and experimental images is obtained with a defocalisation value of 0 nm^{-1} and a thickness of the specimen of 5 nm. The comparison between experimental micrographs (figure 8 (a, c and e)) and simulated images (figures 8 (b, d and f)), is proposed in figure 8.

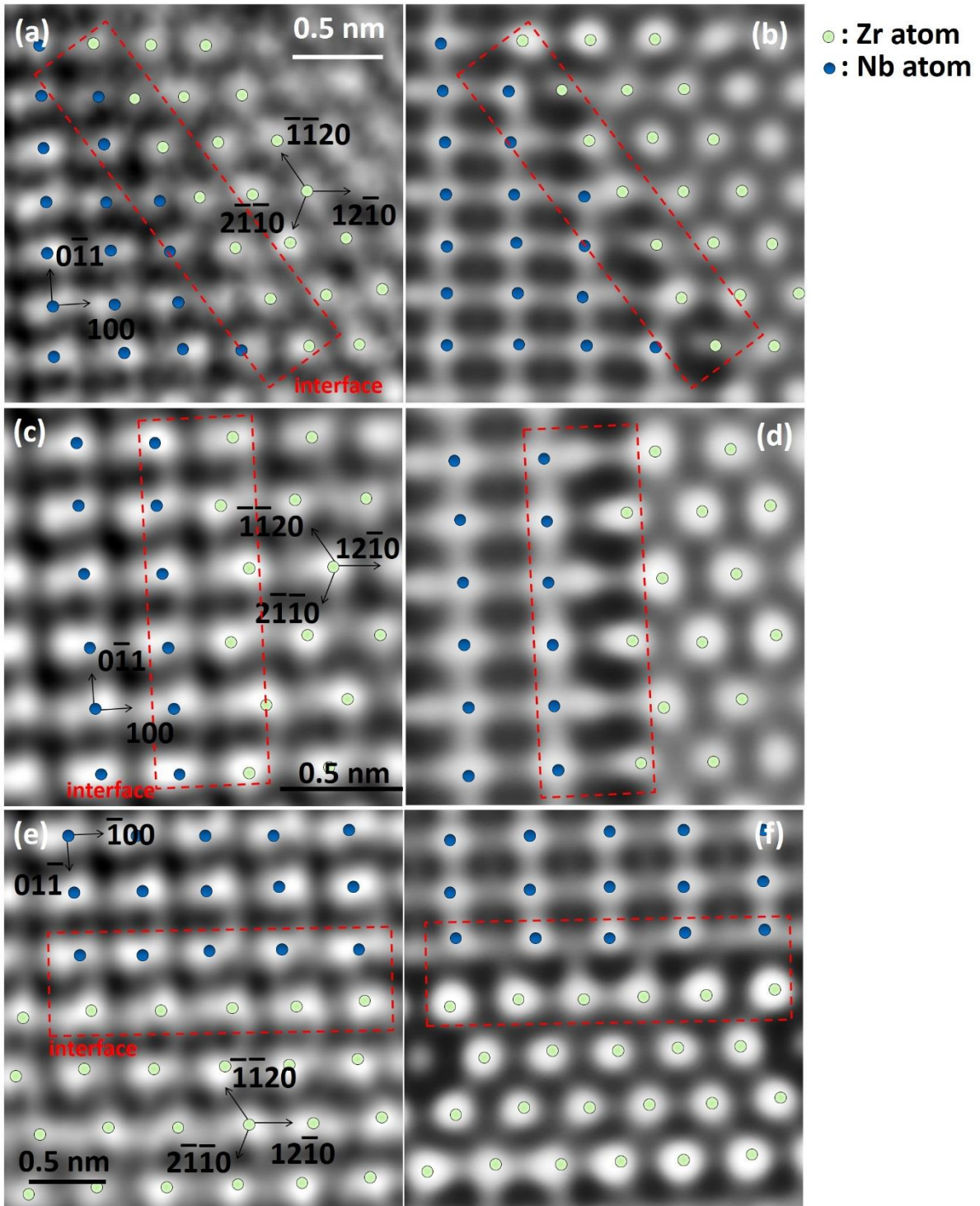**Figure 8:** Comparison between experimental (left) and simulated (right) images : (a) and (b) interface, labelled 1, along the long axis, (c) and (d) interface, labelled 2, at the right part, (e) and (f) interface, labelled 3, at the bottom part.
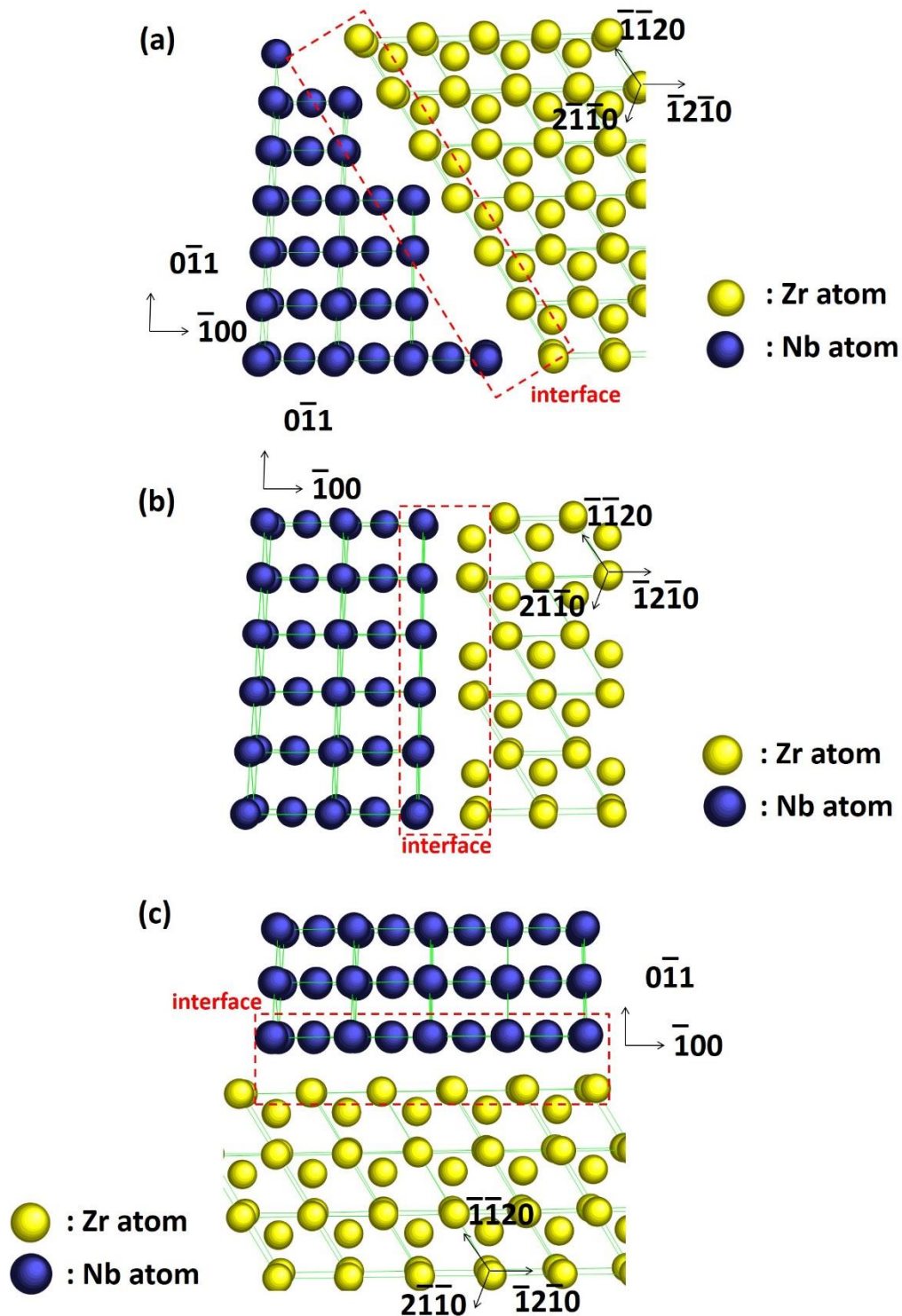
Figure 9: Atomic interface structure of the particle in figure 6: (a) interface 1, along the long axis of the particle, (b) interface 2 at the left part of the particle, (c) interface 3 at the bottom part of the particle.

The long interface of the particle labelled 1 in figure 6 (d), and shown in Figure 8(a) and 9(a), corresponds to the long axis of the particle. This interface lies close to the $[1\bar{1}1]_{Nb}$ and along the $[\bar{1}\bar{1}20]_{Zr}$ directions, which are nearly parallel to each other. In the Nb region, the interface habits an

irrational plane close to the $(\bar{1}\bar{1}1)$, as evidenced by the irregular terrace length, while it habits the $(\bar{1}100)$ plane in the zirconium region. For the niobium side, the interface can be described as a ledged interface with $[0\bar{1}1]$ terraces separated by an array of $[\bar{1}00]$ steps with same height. In the zirconium region, the interface can be described as straight without any step. Due to the ledged interface structure in the Nb side, there is not a perfect atomic row matching since a large number of atoms appear to be out of coincidence across the interface. However, the $(0\bar{1}1)_{Nb}$ and the $(\bar{1}010)_{Zr}$ planes display same interplanar distances which offers continuity across the interface without introduction of dislocations.

Interface labelled 2 in figure 6 (d), shown in figure 8(c) and figure 9(b), corresponds to the right part of the nano-particle. This interface lies along the $[0\bar{1}1]$ direction in the niobium region and along the $[\bar{1}010]$ direction in the zirconium region. In the niobium part, the interface habits the $(\bar{1}00)$ plane and appear clearly straight. In the zirconium part, the interface habits the $(\bar{1}2\bar{1}0)$ plane displays a zig-zag atomic structure. Therefore, along the interface, the atoms are alternatively out and in coincidence since the interface structure corresponds to the particular case where a straight atom row matches a zigzag atom row. An atomic model of the structure of this interface is proposed in figure 9 (b).

Finally, the interface labeled 3 in figure 6 (d), shown in figure 8(e) and figure 9(c), corresponds to the bottom part of the nano-particle. The interface lies along the $[\bar{1}00]$ direction in the Nb region where it habits the $(0\bar{1}1)$ plane and along the $[\bar{1}2\bar{1}0]$ direction in the zirconium region where it habits the $(10\bar{1}0)$ plane. The interfaces corresponds to a straight-to-straight atomic row matching interface, however it offers a large number of out-of-coincidence atoms across the interface and could be classified as incoherent. Figure 9 (c) is an atomic model of this no stepped interface structure.

The comparison between experimental micrographs of the interfaces and simulated images is proposed in figure 8. Figure 10 (a) and (b) are respectively the experimental and simulated images of the zone labelled 1 in figure 6 (d). Figure 10 (c) and (d) are respectively the experimental and simulated images of the zone labelled 2 in figure 6 (d). Figure 10 (e) and (f) are respectively the experimental and simulated images of the zone labelled 3 in figure 6 (d). In a first approximation, the simulated images match well the experimental ones for the three interface configurations. Nevertheless, it has to be kept in mind that other interface configurations are still possible.

Discussion on the Orientation Relationships

The orientation relationship (OR) between two phases of different crystal structures is important because it has a strong bearing on microstructure-property relationships [26]. In Zr-Nb alloy, native b.c.c. beta-Nb precipitates are originally present. But due to the supersaturation of Nb in solid solution in the as-received state, an enhanced precipitation of Nb atoms occurs under neutron irradiation at 623 K. This new precipitation differs from the initial beta-Nb native precipitates since the native precipitates do not seem to have any orientation relationship with the matrix and can be qualified as incoherent [6]. On the other hand, the beta-Nb nano-particles have defined ORs with the matrix. In this paper we reported different ORs and proposed a possible atomic structure configuration of the resulting interfaces.

Experimentally, four ORs between h.c.p. and b.c.c. structure have been observed [26], namely the Burgers OR (0001)//(011), and $[2\bar{1}\bar{1}0]//[1\bar{1}1]$ [28], the Potter OR $(01\bar{1}1)//(110)$ and $[2\bar{1}\bar{1}0]//[1\bar{1}1]$ [29], the Pitsch-Schrader OR (0001)//(011) and $[11\bar{2}0]//[100]$ [30] and the Rong-Dunlop OR (0001)//(021), $(1\bar{1}00)//(0\bar{1}2)$ and $[2\bar{1}\bar{1}0]//[100]$[31]. The reported habit planes corresponding to these OR appear to be irrational in most cases.

In order to predict the most probable orientation relationship between the beta-Nb b.c.c. and Zr h.c.p. crystallographic structure, the edge-to-edge matching model [32] was applied by Zhang et al. [33]. This edge-to-edge model, explained elsewhere [34], considers that the crystallographic properties (i.e. the habit plane and the orientation relationship) of precipitates formed by long-range atom diffusion are governed by the need to minimize the interface energy between precipitate and matrix [34]. According to Shiflet and Merwe [35], the minimum interfacial energy occurs when rows of close packed atoms in the two phases coincide or match at the interface. To achieve the required atom-row matching at the interface a set of planes containing the close packed atom rows in each phase are arranged to meet edge-to-edge in the interface with the atom rows parallel to each other [34].

According to Zhang et al. [33] there are three possible close packed directions for the h.c.p. structure, namely the $\langle 11\bar{2}0\rangle, \langle 10\bar{1}0\rangle$ and $\langle 11\bar{2}3\rangle$. Concerning the b.c.c. structure, there are four possible close packed directions, namely the $\langle 111\rangle$, $\langle 100\rangle$, $\langle 110\rangle$ and $\langle 113\rangle$. The first three are straight atom rows and the last one is zigzag atom row [33]. By considering the interatomic spacing along these directions for lattice structure equal to $a_{Nb}0.33$ nm and $a_{Zr}0.32$ nm, $c_{Zr} = 0.51$ nm, Zhang et al. [33] reported two combinations for the potential matching directions corresponding to the least misfit value. These are: $\langle 11\bar{2}0\rangle/\langle 100\rangle$, and $\langle 10\bar{1}0\rangle/\langle 113\rangle$. Concerning the matching planes, the close packed planes in the h.c.p. structure are $\{0002\}$, $\{10\bar{1}1\}$ and $\{10\bar{1}0\}$. In the b.c.c. structure the close packed planes are $\{110\}$, $\{200\}$ and $\{111\}$. By considering an interplanar distance misfit less than 6% [32], the corresponding matching planes are $\{0002\}/\{110\}$ and $\{10\bar{1}1\}/\{110\}$. By using the Δgs theory [36] to refine these ORs, Zhang et al. [33] obtained the following ORs for beta-Nb precipitates embedded in the Zr matrix:

$[11\bar{2}0]//[100]$, (0002) 3.4° from (011) and $[\bar{1}100]$ 3.4° from $[0\bar{1}1]$ with habit plane $(2\bar{2}05)\sim//(041)$ (1)

$[1\bar{2}10]//[100]$, $(\bar{1}011)$ 4.1° from $(01\bar{1})$ with habit plane close to $(0\bar{2}21)\sim//(11\bar{3})$ (2)

$[2\bar{1}\bar{1}0]$ 0.7° from $[111]$, $(0\bar{1}11)$ 0.8° from $(01\bar{1})$, and $[11\bar{2}0]$ 4.8° from $[00\bar{1}]$ (3).

If we denote by γ the rotation angle between $[\bar{1}100]$ and $[0\bar{1}1]$, then the Burgers OR corresponds to an angle γ = 5.26° while the Pitsch-Schrader OR corresponds to an angle γ = 0°. Hence, the edge-to-edge matching model predicts two ORs (1) and (3) which are close to the Burgers OR since for these ORs, the γ angle is respectively γ = 3.4° and γ = 4.8°.

In our case, the FFT image shown on figure 5 (c) revealed that $[\bar{1}2\bar{1}0]$ is ~2° away from $[\bar{1}00]$, $[\bar{1}010]$ is about ~2° away from the $[0\bar{1}1]$ (hence γ = 2°) and $[11\bar{2}0]$ is ~4° from $[\bar{1}1\bar{1}]$. Thus, the OR reported in our study for the needle shaped particle appears to be in between the Pitsch-Schrader (γ = 0°) and the Burgers (γ = 5.26°) ORs. This result remains anyway in good agreement with the prediction of the edge-to-edge model and also with the result obtained by Luo and Weatherly [37] who reported ORs between beta-Nb and Zr matrix corresponding to γ values between 3.8° and 4.1°. Therefore this OR may be considered as a thermodynamic equilibrium OR that leads to the minimization of the interfacial energy.

Furthermore, if one superimposed the lattice structure of both niobium and zirconium along the $[011]//[0001]$ directions (figure 10), one may find that an invariant line exists between these two structures. The invariant line may be visualized as a row of atoms which is common to both structures. According to the criterion established by Dahmen [25] the rotation angle γ necessary to produce an invariant line between the Zr h.c.p. and the Nb b.c.c. lattice structure, is found to be nearly equal to 4°. In our case, a near invariant line coincides with the $[1\bar{1}1]$ and the $[\bar{1}\bar{1}20]$ crystallographic directions and it is produced for an angle of γ ~2° (figure 12), which remains in good agreement with the prediction of Dahmen [25]. Furthermore, it is worth mentioning that no misfit dislocation is observed along the $[100]/[\bar{1}2\bar{1}0]$ directions and that the $(0\bar{1}1)/(\bar{1}010)$ crystallographic planes matches perfectly since they display an undisrupted continuity. The measure of the $(0\bar{1}1)$ interplanar spacing provides a value $d(0\bar{1}1)$ = 0.27 nm strictly equal to $d(\bar{1}010)$. However, the theoretical $d(0\bar{1}1)$ value is closer to 0.23 nm. One may conclude that the lattice structure of the beta-Nb may be slightly distorted at the interface by elastic effect to ensure a perfect matching of the concerned planes and to produce the invariant line. It is worth mentioning that along the $[100]$ directions the interplanar spacing is still found to be equal to 0.33 nm which corresponds well to the theoretical beta-Nb lattice parameter. This means that the lattice structure is only distorted along the $[0\bar{1}1]$ directions. Thus, the beta-Nb nano-particles display an unrelaxed tetragonal structure rather than a perfect cubic structure owing to interfacial strain effect.
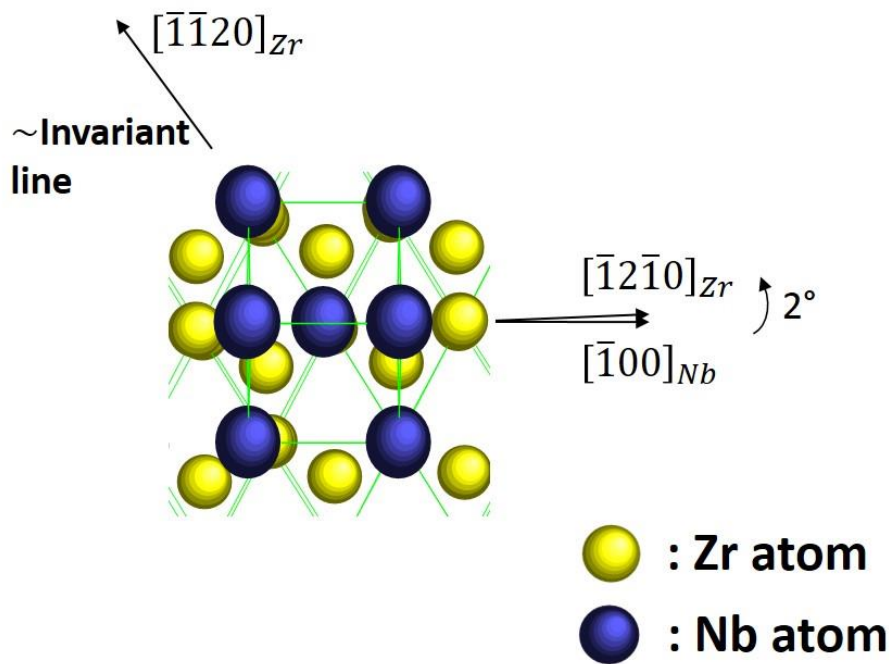
Figure 10: Superimposed Nb and Zr lattice structure oriented along the $[011]//[0001]$ directions and showing a good match in the $[1\bar{1}1]/[\bar{1}\bar{1}20]$ directions producing a near invariant line.

From this analysis, the shape of the studied particle can be explained. Indeed, the long direction of the nano-particle is parallel to the $[\bar{1}\bar{1}20]$ direction and nearly parallel to the $[1\bar{1}1]$ direction which corresponds well to the invariant line and thus to the direction of low mismatch. This explains why the particle exhibits an elongated shape along the invariant line. According to Dahmen [26], the needle shape exclusively appears for a rotation angle γ which is less than 5.26°. Therefore, with a rotation angle of γ = 2°, the needle shape of the observed particle (figure 6 (a)) is consistent with the statement of Dahmen [26] .

It should however be pointed out that there are probably other types of orientation relationships between the Zr matrix and the beta-Nb nano-precipitates. A statistical study done on many particles would be required to have a better knowledge and understanding of the shape of these particles. Furthermore, the reason for the very thin thickness of the particle along the <c> direction remains not known. More high resolution TEM observations associated with atomic scale computations would be required to really understand the origin of the shape of these beta-Nb nano-particles.

Conclusion

In neutron irradiated Zr-Nb alloy, the beta-Nb particles have the 3D geometry of small parallelepiped close to a needle shape (or flattened rice grain), with the long direction (6 nm) and the width (3 nm) which are in the basal plane and the short thickness (1.5 nm) being along the <c> axis. We reported that the needle shaped beta-Nb particles display an orientation relationship in between the Pitsch-Schrader and the Burgers orientation relationships. Such orientation offers three distinct interface configurations at respectively the needle length, the bottom-left (right) part and the bottom part of the particle. A precise description of the atomic interface structures between the b.c.c. niobium crystal and the h.c.p. zirconium crystal has been proposed at these three regions. Furhermore, it is shown that the beta-Nb nano-particles display an unrelaxed tetragonal structure rather than a perfect cubic structure owing to interfacial strain effect. The elongated shape of the particle, in the basal plane, has been explained by the existence of an invariant line along the [1120] type direction.

References

[1] K.N. Choo, Y.H. Kang, S.I. Pyun, V.F. Urbanic, Effect of composition and heat treatment on the microstructure and corrosion behavior of Zr-Nb alloys, J. Nucl. Mater. 209 (1994) 226-235

[2] C. Lemaignan, Compr Nucl Mater., 2012

[3] J.P. Mardon, D. Charquet, and J. Senevat, Influence of composition and fabrication process on out-of-pile and in-pile properties of M5 alloy, 12th Int. Symp. on Zr in the Nuclear Industry, ASTM STP 1354 (West Conshohocken, PA:, ASTM, 2000), pp. 505–524.

[4] P. Barberis, D. Charquet, V. Rebeyrolle, Ternary Zr–Nb–Fe(O) system: phase diagram at 853 K and corrosion behaviour in the domain Nb < 0.8%, J. Nucl. Mater. 326 (2004) 163-174

[5] V.N. Shishov, A. V. Nikulina, V.A. Markelov, M.M. Peregud, A. V. Kozlov, S.A. Averin, S. A. Kolbenkov, A.E. Novoselov, Influence of neutron irradiation on dislocation structure and phase composition of Zr-base alloys, Zirconium in the Nuclear Industry: Eleventh International Symposium, ASTM STP 1295, E.R. Bradley and G.P. Sabol, Eds, American Society for testing and materials, 1996, pp. 603-622

[6] S. Doriot , D. Gilbon , J-L. Bechade , M-H. Mathon , L. Legras , and J-P. Mardon : Microstructural stability of M5™ Alloy irradiated up to high neutron fluences. J. ASTM Int. 2(7), 175 (2005).

[7] C. Toffolon-Masclet, P. Barberis, J.C. Brachet, J.P. Mardon, L. Legras, Study of Nb and Fe precipitation in alpha-phase temperature range (400 to 550°C) in Zr-Nb-(Fe-Sn) alloys, J. ASTM Int. 2(5), 81 (2005).

[8] RW Gilbert, K Farrel, CE Coleman, Damage structure in zirconium alloys neutron irradiated at 573 to 923 K, J. Nucl. Mater. 84 (1979) 137-148

[9] V. Perovic, A. Perovic, G.C. Weatherly, L.M. Brown, G.R. Purdy, R.G. Fleck, R.A. Holt, Microstructural and microchemical studies of Zr-2.5 Nb pressure tube alloy, J. Nucl. Mater. 205 (1993) 251-257

[10] S. Doriot, B. Verhaeghe, J.-L. Béchade, D. Menut, D. Gilbon, J.-P. Mardon, J.-M. Cloué, A. Miquet, L. Legras, Microstructural Evolution of M5^{TM} Alloy Irradiated in PWRs up to High Fluences— Comparison With Other Zr-Based Alloys, Zirconium in the Nuclear Industry: 17th International Symposium, ASTM STP 1295, R. Comstock and P. Barberis, Eds, American Society for testing and materials, 2013, pp. 759-799

[11] J.L Béchade, D. Menut, S. Doriot, S. Schlutig, B. Sitaud, X-ray diffraction analysis of secondary phases in zirconium alloys before and after neutron irradiation at the MARS synchrotron radiation beamline, J. Nucl. Mater. 437 (1) (2013) pp. 365-372

[12] D. Menut, J.L. Béchade, S. Cammeli, S. Schlutig, B. Sitaud, P.L. Solari, Synchrotron radiation investigations of microstructutral evolutions of ODS steels and Zr-based alloys irradiated in nuclear reactors, J. Mater. Res. 30 (9) (2015), pp. 1392-1402

[13] C.E. Coleman, R.W. Gilbert, G.J.C. Carpenter, G.C. Weatherly, Proceedings of a Symposium on Phase Stability during Irradiation, The Metallurgical Society of AIME. Pittsburgh. PA. 5-9 Oct. 1980

[14] C.E. Coleman, R.W. Gilbert, G.J.C. Carpenter, G.C. Weatherly, Proceedings of a Symposium on Phase Stability during Irradiation, The Metallurgical Society of AIME. Pittsburgh. PA. 5-9 Oct. 1980

[15] Shishov, V.N., Peregud, M.M., Nikulina, A.V., Pimenov, Yu. V, Kobylyansky, G.P., Novoselov, A.E., Ostrovsky, Z.E. and Obukhov, A.V." *Zirconium in the Nuclear Industry: 14th International Symposium*, ASTM STP 1467, ASTM International, West Conshohocken, PA, 2005, pp. 666-685

[16] H. Okamoto, Nb-Zr (Niobium-Zirconium), Journal of Phase Equilibria, 13(5) (1992) p.577

[17] J.P. Abriata, J.C. Bolcich, The Nb-Zr (Niobium-Zirconium) system, Journal of Phase Equilibria, 3(1) (1982), pp. 34-44

[18] A. Sarce, Stability of precipitates in the anisotropic α-Zr matrix under irradiation, J. Nucl. Mater. 185 (1991) p.214

[19] S.I. Maydet, K.C. Russel, Precipitate stability under irradiation: Point defect effects, J. Nucl. Mater. 64 (1977) p. 101

[20] A. A. Turkin, A. V. Buts, A. S. Bakai, Construction of radiation-modified phase diagrams under cascade-producing irradiation: application to Zr-Nb alloy, J. Nucl. Mater. 305 (2002) 134-152.

[21] J. Ribis, F. Onimus, J-L. Béchade, S. Doriot, C. cappelaere, C. Lemaignan, A. barbu, O. rabouille, Experimental and modeling approach of irradiation defects recovery in zirconium alloys : impact of an applied stress, J. ASTM Int. 5(3), 81 (2008), 1-21

[22] J. Ribis, F. Onimus, J-L. Béchade, S. Doriot, A. barbu, C. cappelaere, C. Lemaignan, Experimental study and numerical modelling of the irradiation damage recovery in zirconium alloys, J. Nucl. Mater. 403 (2010) 135-146

[23] B. Bourdiliau, F. Onimus, C. Cappelaere, V. Pivetaud, P. Bouffioux, V. Chabretou, A. Miquet, Impact of irradiation damage recovery during transportation on the subsequent room temperature tensile behavior of irradiated zirconium alloys, J. ASTM Int. 7(9) (2011) 929-953

[24] P. Stadelman, Microsc. Microanal. 9 (2003) 60-61

[25] Kilaas R. http://www.totalresolution.com/

[26] U. Dahmen, Orientation relationships in precipitation systems, Acta Metallurgica, vol. 30, (1982) 63-73

[27] D. Duly, Application of the invariant line model for bcc/hcp couples: A criterion based on surface variations, Acta Metall. Mater. 1993;41:1559

[28] Burgers W.G., On the process of transition of the cubic-body-centered modification into the hexagonal-close-packed modification of zirconium, Physica 1934;1:561

[29] Potter D.I., J. Less-common Metals, 1973;31:299

[30] Pitsch W., Schrader A., Arch Eisenhütt Wes 1958;29:715

[31] Rong W., Dunlop GL., The crystallography of secondary carbide precipitation in high speed steel, Acta Metall. 1984;32:1591

[32] P.M. Kelly, M.-X. Zhang, Edge-to-edge matching-a new approach to the morphology and crystallography of precipitates, Mater. Forum, 1999, vol. 23, pp. 41-62

[33] M.-X. Zhang, P.M. Kelly, Edge-to-edge matching and its applications Part I. Application to the simple HCP/BCC system, Acta mater. 53 (2005) 1073-1084

[34] P.M. Kelly, M.-X. Zhang, Edge-to-edge Matching- The fundamentals, Metall. Mater. Trans. A, vol. 37A, (833-839), 2006

[35] G.J. Shiflet, J.H. Van der Merwe, The role of structural ledges as misfit-compensating defects: fcc-bcc interphase boundaries, Metall. Mater. Trans. A, 1994, vol. 25A, pp. 1895-1903

[36] W.Z. Zhang, G.R. Purdy, A TEM study of the crystallography and interphase boundary structure of α precipitates in a Zr-2.5 wt% Nb alloy, Acta Metall. Mater., 41 (1993) 543

[37] C.P. Luo, G.C. Weatherly, The precipitation behavior of a Zr-2.5 wt pct Nb alloy, Metall Trans A (1998) 19 p1153-1162